Direct Current Electrodeposition of Zn-SiC Nanocomposite Coatings from Citrate Bath

Honorata Kazimierczak,[1,*,z] Krzysztof Szymkiewicz,[1] Łukasz Rogal,[1] Eliezer Gileadi,[2,] and Noam Eliaz[3,*]**

[1] *Institute of Metallurgy and Material Science, Polish Academy of Sciences, 30-059 Krakow, Poland*
[2] *School of Chemistry, Faculty of Exact Sciences, Tel-Aviv University, Ramat Aviv 6997801, Israel*
[3] *Biomaterials & Corrosion Laboratory, Department of Materials Science and Engineering, Tel-Aviv University, Ramat Aviv 6997801, Israel*

Zn-SiC nanocomposite coatings are successfully produced by galvanostatic electrodeposition from aqueous citrate solutions, using SiC nanoparticles (NPs) with an average size of 56 nm. The optimal parameters of the zinc-citrate bath are chosen on the basis of analysis of a thermodynamic model. The effect of applied current density, bath composition, and hydrodynamic conditions are studied. The kinetics and mechanism of zinc reduction in the presence of SiC NPs are investigated using cyclic voltammetry. The surface charge of SiC NPs suspended in the electrolyte solutions is examined by the dynamic light scattering technique. The electrodeposited Zn-SiC coatings are characterized by wavelength dispersive X-ray fluorescence and scanning electron microscopy. It is shown that SiC codeposition with Zn proceeds through the entrapment of ceramic NPs during the reduction of citrate-zinc ions that are first adsorbed on the surface of the ceramic NPs. A maximal content of 6.4 wt% SiC incorporated into the Zn matrix is obtained at the lowest applied current density of $j = -0.5$ A dm^{-2}, with a nearly constant faradaic efficiency of 90%.
 [DOI: 10.1149/2.0421811jes]

Manuscript submitted June 14, 2018; revised manuscript received August 2, 2018. Published August 16, 2018.

Electrodeposition is an attractive process for forming metal-matrix composite (MMC) coatings thanks to its simplicity, versatility, scale-up capability, ability to coat parts with complex geometries, and low cost. Furthermore, it is a non-line-of-sight process that can be conducted at ambient temperature and pressure, and can yield good strength of adhesion between the coating and the substrate. The fabrication of nano-composite coatings can be achieved via electrochemical deposition of the matrix material (e.g. metal, alloy, semiconductor, or conducting polymer) from a solution in which insoluble ceramic powders are dispersed. These composite coatings can offer substantial improvement of a variety of properties, such as hardness and strength, wear and corrosion resistance, self-lubrication, high-temperature performance, and chemical or biological compatibility.[1–5]

A variety of ceramic particles have been incorporated into electrodeposits, including Al_2O_3, TiO_2, ZrO_2, Cr_2O_3, MoS_2, WC, diamond, and SiC. SiC provides high wear, temperature, thermal shock, and corrosion resistance. It is chemically inert in all alkaline and acid solutions, and has superior hardness. Electrodeposition of MMCs with SiC reinforcement has already been widely studied, mainly with Ni matrices.[5–16] Zinc-based coatings are widely used for cathodic protection of steels from corrosion, due to their low cost and environment compatibility.[1] Zinc, however, has low hardness and low abrasion resistance, which can be improved by its reinforcement with ceramic particles. Yet, there are only few articles dealing with electrodeposition of Zn–SiC systems.[17–26]

The microstructure and properties of electrodeposited MMCs with ceramic particle reinforcement are affected by the particle chemistry, size, concentration, dispersion quality, and incorporation rate, as well as by the applied current/potential value and profile, pH, the presence of additives, temperature, and bath stirring. The incorporation of the inert particles into the deposit has been enhanced by high particle concentration, low electroactive species concentration, smaller-size particles, and pulsed current/potential.[20–22,25,26]

SiC has been found to shift the reduction potential of zinc and hydrogen ions to more positive potentials, with an increase in both partial current densities.[18–20] Several hypotheses have been made to explain such effects of the inert particles on cathodic reactions: increase in cathode surface area due to the adsorbed particles,[27] change in texture promoted by the particles,[28] migration component,[27] and turbulent flow promoted by the particles.[29] Tulio and Carlos[19] suggested that SiC may be regarded as an additive that promotes Zn electrodeposition from acidic solutions. It has also been reported that SiC suspended in an aqueous solution is covered by a few nanometer thick layer of silica (SiO_2). Yeh and Wan[30] found the point of zero charge (PZC) of SiC to be at pH = 2.2, while Drzymała[31] characterized SiC as being hydrophobic.

Although significant effort has been made on electrodeposition of MMCs reinforced with ceramics, the mechanism of particle incorporation from suspension is not yet well understood. Several theories have been proposed, including electrophoresis, mechanical entrapment, adsorption, and convective-diffusion,[26] since Guglielmi first introduced his model of two successive adsorption steps.[32] The latter model was later expanded[33] to the Co–SiC system, relating weight percent of embedded particles to current density for different suspension particle concentrations. A mathematical model of the incorporation of SiC particles into a codeposited Ni film on a rotating disk electrode (RDE) was proposed by Eroglu and West.[34] According to this model, the particles are transported to the electrode surface, adsorb onto it, and are incorporated if the residence time of any individual particle on the electrode is sufficient to allow burial in the codeposited Ni. The rate of incorporation is thus proportional to the residence time, inversely proportional to the burial time, and is proportional to the number density of particles on the surface. These times are influenced by the hydrodynamics, particle size, current density, and concentration of dispersants used to stabilize the particles. Obviously, the use of each of the above theories is limited to specific experimental conditions.

The objective of this work is to study the electrodeposition of Zn–SiC composite layers from aqueous citrate-based electrolytes. The effects of applied current density, electrolytic bath composition, and hydrodynamic conditions are investigated in order to understand the kinetics and mechanism of the electrode processes taking place during codeposition of SiC with Zn from these electrolytes.

Materials and Methods

The plating baths were prepared by dissolving sodium citrate (0.25 M) and zinc sulfate (0.20 M) in deionized water, followed by the addition of SiC nanoparticles (NPs) together with gelatin (1 g L^{-1}) as a surfactant. The pH was adjusted to 4.5 by the addition of sulfuric acid. All chemicals used were of analytical grade. The spherical SiC NPs were supplied by Nanostructured & Amorphous Materials, Inc. (Houston, TX), and had an average size of 56 nm. The solutions

*Electrochemical Society Member.
**Electrochemical Society Fellow.
[z]E-mail: honorata.kazimierczak@gmail.com

were stirred magnetically for 24 h at 200 rpm before electrochemical deposition, in order to disperse the particles. All experiments were conducted at room temperature.

A thermodynamic model of the distribution of species in the Zn–Cit system was constructed on the basis of stability constants from the appropriate databases.[38–41] Some additional stability constants were determined by Ozga et al.[42–44] The model calculations were run using the HYDRA and MEDUSA programs.[45]

The electrochemical measurements were performed in a 200 cm^3, three-electrode cell with a RDE, to ensure constant hydrodynamic conditions. An Ametek ParSTAT263A and a Metrohm Autolab PGSTAT302N potentiostats/galvanostats were used for cyclic voltammetry (CV) and electrodeposition, respectively. The working electrode was a copper disc placed in a sealed Teflon holder (active surface area of 2.83 cm^2). A platinum sheet (3.5 cm^2) was used as a counter electrode. All potentials were measured versus a saturated calomel electrode (SCE). The same scan rate of 35 mV s^{-1} was used in all voltammetry measurements, in which the potential scan was started in the negative direction, from –0.15 V vs. SCE.

Electrochemical impedance spectroscopy (EIS) measurements were carried out using a Bio-Logic SAS' VSP multichannel potentiostat/galvanostat in a three-electrode Flat Cell having a volume of 250 mL. The area of the working electrode was 1 cm^2. A Pt mesh and a saturated Ag/AgCl (3 M KCl) electrode (+0.210 V vs. SHE) were used as the counter and reference electrodes, respectively. EIS measurements were conducted in the potential range from –0.3 V to +0.3 V versus open-circuit potential (OCP). A superimposed perturbation of 10 mV and a frequency range of 60 kHz to 10 mHz were used. The double-layer capacitance C_{dl} was determined by fitting a simple Randles equivalent circuit.[1]

The composition of deposits was determined by wavelength dispersive X-ray fluorescence (WDXRF). Analysis was carried out using a Rigaku Primini spectrofluorimeter with scintillation counters (LiF crystal). The weight percentage of SiC in the Zn–SiC composite was then calculated from the Zn and Si weight percentages, using Eq. 1:[20]

$$\mathrm{SiC\,(wt\%)} = \frac{\mathrm{Si\,(wt\%)} + \frac{\mathrm{Si(wt\%)}}{M_{Si}} \times M_C}{\mathrm{Zn\,(wt\%)} + \mathrm{Si\,(wt\%)} + \frac{\mathrm{Si(wt\%)}}{M_{Si}} \times M_C} \times 100 \qquad [1]$$

where M_{Si} and M_C are the atomic masses of silicon and carbon, respectively. The current efficiency of the process was calculated according to Eq. 2:[12]

$$\eta\ (\%) = \frac{m_{Zn(r)}}{m_{Zn(t)}} = \frac{\Delta m - \mathrm{SiC\,(wt\%)} \times \Delta m}{k_{Zn} Q} \times 100 \qquad [2]$$

where $m_{Zn(r)}$ is the real mass of the deposited zinc matrix, $m_{Zn(t)}$ is the theoretical mass of deposited zinc calculated from Faraday's law, Δm is the mass of the deposited composite (Zn-SiC) layer, k_{Zn} is the electrochemical equivalent of Zn (3.39×10^{-4} g C^{-1}), and Q is the charge applied during electrodeposition (= It). The Zn deposition rate was calculated from the known deposition time and the mass of deposits (subtracting the mass of SiC incorporated into Zn). The samples were weighed before and after deposition using Kern ALT analytical scales with a readability of 0.01 mg. The reproducibility of the electrodeposition process was verified using three to five replicates; typical results are reported herein.

The zeta (ζ) potential of SiC NPs suspended in citrate-based electrolytes was measured using a Zetasizer Malvern ZS system. The zeta potential was obtained from the electrophoretic mobility by the Smoluchowski equation.[46] The surface morphology and the cross-section of the Zn–SiC composite coatings were characterized by a FEI model Quanta 3D field-emission gun (FEG) scanning electron microscope (SEM), equipped with an energy-dispersive X-ray spectroscopy (EDS) Trident system (Apollo 40 EDS spectrometer).

Results and Discussion

Determination of the optimal electrolyte solution.—Aqueous citrate-based solutions were used for electrodeposition of Zn–SiC composite coatings, because they are non-toxic and form strong complexes with Zn(II). These solutions provide stable pH values in the range of 4.0–6.0 and are widely used in the electrodeposition of zinc and its alloys.[47–49] The concentration of the electroactive zinc citrate complexes depends on the citrate content in the solution.[42,50] The concentration of sodium citrate in the electrolyte solution should be equal to, or slightly higher than, the concentration of the deposited metal ions.[51] Hence, the concentrations of zinc and citrate ions were 0.20 M and 0.25 M, respectively. The optimal pH value was defined as 4.5, at which the highest concentration of electroactive $Zn(HCit)^-$ exists. The concentration of the non-electroactive $Zn(HCit)_2^{4-}$ is much lower, and increases greatly as the pH is increased, as shown in Fig. 1. Also, the H_3Cit concentration is low at pH = 4.5, ensuring a relatively low rate of hydrogen evolution.

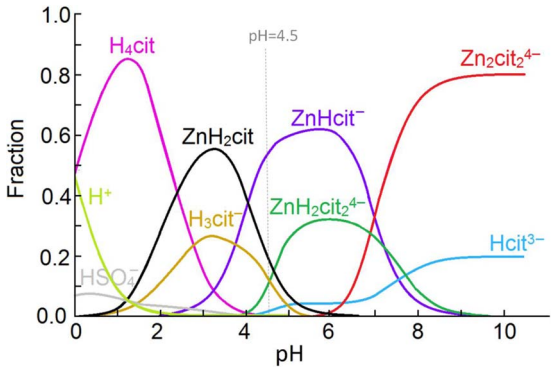

Figure 1. The distribution of species in the Zn–Cit system as a function of the pH of a solution containing 0.25 M Na_3HCit and 0.20 M $ZnSO_4$. The gray dotted line marks the pH of the solution used in this work.

Electrode reactions in the Zn–Cit system.—Reactions 3 through 10 list the reduction reactions that may take place in the Zn–Cit system:[42,43,51]

$$Zn^{2+} + 2e^- \rightarrow Zn^0 \qquad -1.001\ \mathrm{V} \qquad [3]$$

$$Zn(HCit)^- + H_2O + 2e^- \rightarrow Zn^0 + H_2Cit^{2-} + OH^- \qquad -1.465\ \mathrm{V} \qquad [4]$$

$$ZnH_2Cit^0 + 2e^- \rightarrow Zn^0 + H_2Cit^{2-} \qquad -1.171\ \mathrm{V} \qquad [5]$$

$$2H^+ + 2e^- \rightarrow H_2 \qquad -0.242\ \mathrm{V} \qquad [6]$$

$$H_4Cit^0 + 2e^- \rightarrow H_2 + 2H_2Cit^{2-} \qquad -0.525\ \mathrm{V} \qquad [7]$$

$$H_3Cit^- + 2e^- \rightarrow H_2 + HCit^{3-} \qquad -0.555\ \mathrm{V} \qquad [8]$$

$$2H_2Cit^{2-} + 2e^- \rightarrow H_2 + 2HCit^{3-} \qquad -0.503\ \mathrm{V} \qquad [9]$$

$$2H_2O + 2e^- \rightarrow H_2 + 2OH^- \qquad -1.069\ \mathrm{V} \qquad [10]$$

All voltages listed above are the standard potentials versus SCE. The reduction of zinc according to Reaction 3 can be excluded, because the studied Zn–Cit bath at pH = 4.5 contained zinc mostly bound in the form of citrate complexes (Fig. 1). Hence, zinc electrodeposition most likely proceeds through the reduction of $Zn(HCit)^-$ (Eq. 4) and ZnH_2Cit^0 (Eq. 5), while the more negative $Zn(HCit)_2^{4-}$ present in the bath (Fig. 1) was proved to be non-electroactive,[42,43] hence its reduction to zinc does not take place. The reduction of hydrogen according to Eq. 6 is negligible because of the negligible amount of

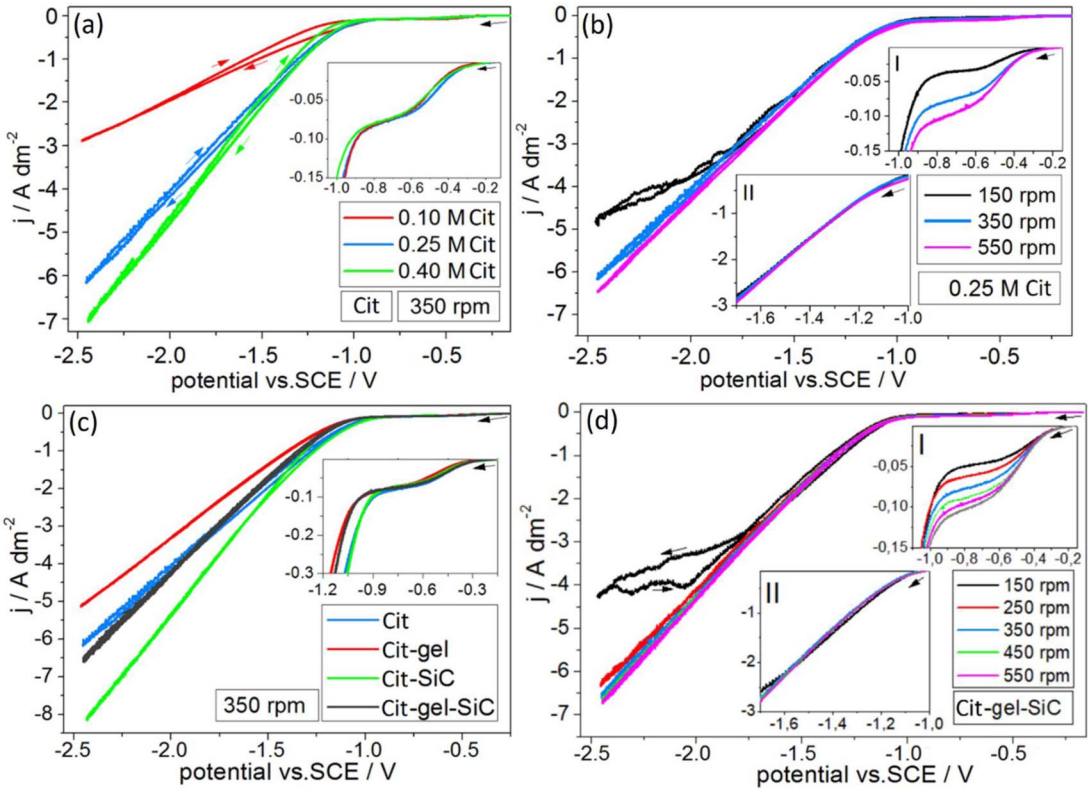

Figure 2. Cyclic voltammograms measured on a Cu substrate. Cit and Cit–SiC systems, with and without gelatin addition, scan rate = 35 mV s^{-1}, $T = 20°C$. Arrows indicate scan direction. The insets provide zoom-in to selected regions.

free hydrogen ions in the electrolyte studied (Fig. 2), while hydrogen evolution related to the decomposition of water (Eq. 10) is expected to occur only at very high overpotentials.

Hydrogen evolution by deprotonation of the carboxylate groups of citrate ions seems to be essential in the whole range of current/potential values considered (Eqs. 7–9). The hydroxyl group present in the $HCit^{3-}$ ion (Fig. 1) could theoretically also be the proton donor. However, it is generally considered that the hydroxyl group deprotonates only at highly alkaline pH values, estimated to be between 11 and 14.4;[52–57] hence, it is not considered herein. Eq. 7 may also be disregarded due to the lack of H_4Cit ions in the investigated electrolyte solution at pH = 4.5 (Fig. 1).

In summary, it can be argued that in the studied Zn–Cit-based systems, zinc electrodeposition proceeds according to Eqs. 4 and 5, whereas hydrogen evolution proceeds mainly via the deprotonation of H_3Cit^- and H_2Cit^{2-} complex ions (Eqs. 8 and 9, respectively).

Voltammetric investigation in Zn–Cit-based systems, with or without suspended SiC nanoparticles.—Cyclic voltammograms were measured in order to analyze the influence of suspended SiC NPs on the electrode processes occurring in aqueous zinc-citrate solutions (Figs. 2 and 3). In all cases, rising of the cathodic current density starts at –0.30 V vs. SCE, and a limiting current (plateau) is observed in a relatively small current range of 0.05–0.12 A dm^{-2}. Taking into account the standard potentials listed above and the low reaction rate reflected from this limiting current, it may be assumed that hydrogen evolution from free hydrogen ions (Eq. 6) is the related reaction. The amount of these ions is negligible according to Fig. 1, and indeed is very small, but still noticeable in the CVs. Next, a sharp increase of cathodic current density starts at –0.9 V. The current density rises linearly with further shift of potential toward more negative values. The registered cathodic current density increases when the citrate concentration in the electrolyte is increased (Fig. 2a). Hence, this part of the CV represents hydrogen evolution from citrate ions, Eqs. 8 and 9, which is enhanced as the concentrations of $Zn(HCit)^-$ and ZnH_2Cit^0 species in the electrolyte are increased. These reactions are independent of the hydrodynamic conditions, and hence are activation-controlled at potentials up to about –1.7 V vs. SCE and the related current density of about –3.0 A dm^{-2} (Fig. 2b, inset II). At higher polarization, hydrogen evolution becomes mass-transport-controlled; it grows with the increase of rotation rate of the disc cathode (Fig. 2b). In this range of current-potential, hydrogen evolution becomes intense: gas bubbles are observed on the cathode surface, and at the lowest RDE speed applied (150 rpm) they block the surface of the working electrode. The latter phenomenon is reflected in the CV by its irregularity and relatively small current density under such conditions. Higher RDE speeds ensure sweeping of hydrogen gas bubbles from the surface of the working electrode and continuity of reduction processes; hence, the voltammograms are smoother, and higher cathodic current densities are registered (Fig. 2b). The lack of any anodic peak and clean surface of copper confirms that hydrogen evolution is the only process occurring under the chosen conditions.

Next, the effect of the addition of either SiC NPs or gelatin on the electrode processes was studied (Fig. 2c). Neither gelatin nor SiC changes the course of the reduction of free hydrogen ions (Fig. 2c, inset), while both influence noticeably the kinetics of hydrogen evolution from citrate ions. Generally, the addition of gelatin inhibits the reduction reaction (probably, by the adsorption on the cathode surface). Gelatin is a hydrolysed form of collagen, which is sometimes added to electroplating baths (e.g., in zinc electrodeposition[58]) to control the deposition rate, crystallization, leveling, and brightness of the deposit. Previously, Eliaz et al.[59] reported that gelatin changes the phase content in Zn–Ni, Zn–Co and Zn–Ni–Co alloys as a result of its adsorption on the surface of the cathode. In that case, the change in the CV was also reflected by a shift of the deposition potential to a slightly less negative value and a decrease in the deposition current density.

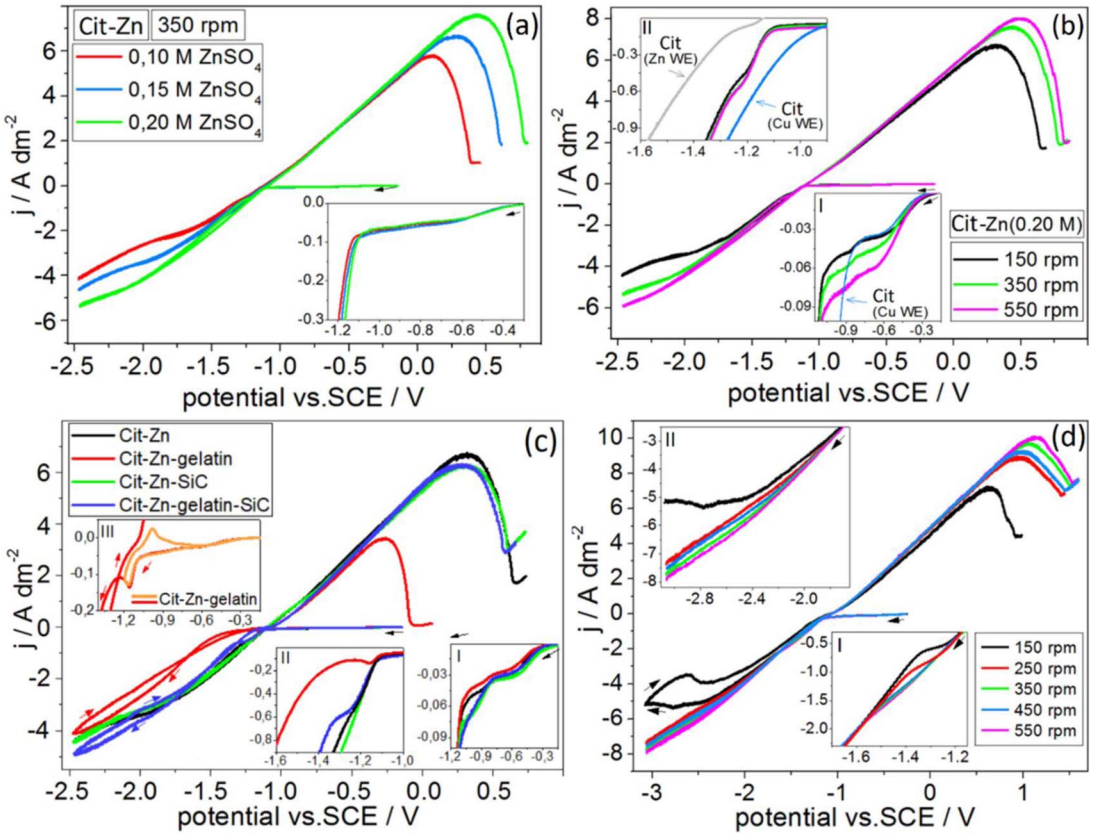

Figure 3. Cyclic voltammograms measured on a Cu substrate. Zn–Cit and Zn–Cit–SiC systems, with and without gelatin addition, scan rate = 35 mV s^{-1}, T = 20°C. Arrows indicate scan direction. The insets provide zoom-in to selected regions. The gray and blue lines in Fig. 3b, inset II, represent voltammetric curves registered in Cit system on Zn and Cu electrodes, respectively. The orange line in Fig. 3c is a voltammogram obtained in Zn–Cit–gelatin system in the smaller potential range (the vertex potential is $E_V = -1.2$ V).

On the other hand, the addition of SiC NPs to the Cit and Cit–gelatin systems enhances the kinetics of hydrogen evolution associated with the reduction of citrate ions (Figs. 2c). The simultaneous presence of gelatin and SiC NPs in the citrate-containing electrolyte results in the electrode kinetics being very close to the one observed in a pure citrate bath (Figs. 2c, 2d). The effect of RDE speed on electrode kinetics in the Cit–gel–SiC system is presented in Fig. 2d. This figure confirms the same trend observed in the citrate system, namely, at low RDE (150 rpm) and high polarization (up to –1.7 V vs. SCE), strong inhibition of the electrode processes is observed. This inhibition may be related to blockage of the cathode surface by hydrogen gas bubbles remaining on its surface. Furthermore, the current density registered in the presence of suspended SiC NPs is even smaller than the one observed in pure citrate bath under the same conditions, which suggests that SiC NPs may also block the electrode surface.

Next, the electrodeposition of zinc is analyzed (Fig. 3). Zinc reduction starts at a potential of about –1.15 V vs. SCE (Fig. 3a, inset), and the cathodic current density increases apparently with the shift of potential toward negative values. The anodic peak associated with the oxidation of previously deposited zinc starts at about –1.05 V vs. SCE, and its height grows with the increase of zinc sulfate in the electrolyte (Fig. 3a), as well as with the increase of RDE speed (Fig. 3b). A careful inspection of the cathodic part of the CVs obtained in the Zn–Cit system (Fig. 3b, insets I and II) allows to notice an overlapping effect of hydrogen evolution and zinc deposition under the conditions studied. Namely, the beginning of hydrogen evolution from citrate ions can be noticed as a curvature at 0.9 V vs. SCE (Fig. 3b, inset I). It represents hydrogen evolution on the surface of the copper substrate. Next, after a sharp increase of cathodic current density, associated with the beginning of zinc deposition, another bending of the voltammetric curve is observed at –1.2 V and a related current density of about –0.6 A dm^{-2} (Fig. 3b, inset II). It can be explained again as a beginning of hydrogen evolution due to reduction of citrate ions, albeit this time on the zinc surface. Such hypothesis is in line with the course of hydrogen evolution on the zinc surface in pure citrate electrolyte (gray line in inset II of Fig. 3b).

The presence of SiC NPs in the Zn–Cit system does not seem to change considerably the kinetics of electrode reaction compared to pure Zn–Cit electrolyte. On the other hand, the addition of gelatin results in significant inhibition of the zinc deposition reaction (Fig. 3c). The start of zinc deposition at about –1.15 V is followed by the immediate adsorption of gelatin on the cathode surface, which results in the formation of a characteristic cathodic peak in the CV (Fig. 3c, inset III). The anodic peak associated with the oxidation of previously deposited zinc is observed in the voltammogram with a vertex potential $E_v = -1.2$ V (Fig. 3, inset III, orange line), thus confirming that the discussed cathodic peak is associated with Zn deposition. Next, a notably lower anodic peak of zinc oxidation in the Zn–Cit–gel system, as compared to other Zn-Cit systems considered (Fig. 3c), confirms the gelatin inhibition effect. Further addition of SiC to the Zn–Cit–gel system results in the enhancement of the rate of zinc deposition, as evident from the observed cathodic current density as well as the height of the anodic peak – similar to those observed in the Zn–Cit and Zn–Cit–SiC systems. The cathodic region, with a characteristic bending starting at –1.2 V vs. SCE (–0.6 A dm^{-2}), is clearly more pronounced in the case of Zn–Cit–SiC–gel (Fig. 3c, inset II) in comparison to Zn–Cit (Fig. 3b, inset II). This is related to the shift in the reduction potential of citrate ions on zinc due to adsorption of gelatin (Fig. 2c, inset). Moreover, as evident in inset I of Fig. 3c, the rate of hydrogen evolution due to reduction of citrate ions (starting at –0.9 V vs. SCE) is also promoted in the presence of suspended SiC NPs, both in the Zn–Cit and in the Zn–Cit–gel systems.

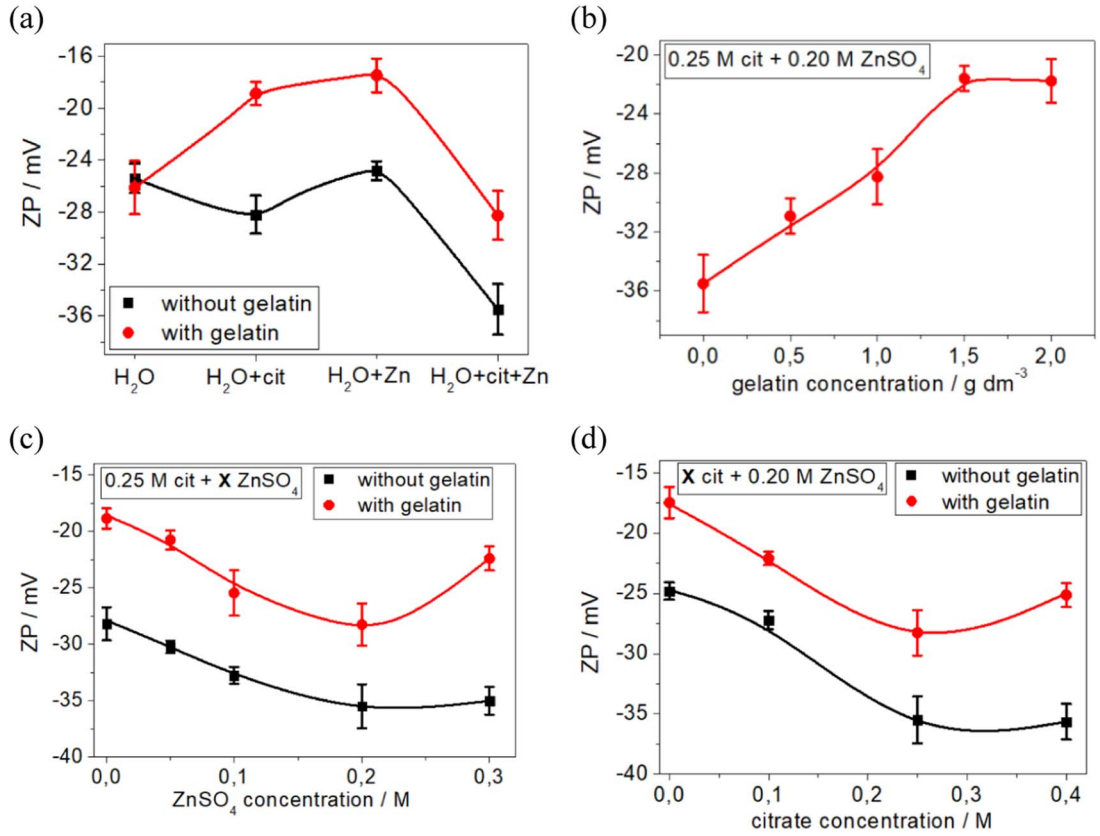

Figure 4. (a) Zeta potential (ZP) of SiC nanoparticles in a water-based solution containing zinc (0.20 M) and citrate (0.25 M) ions, either separately or together, with and without addition of 1 g dm^{-3} gelatin. The dependence of zeta potential on (b) concentration of gelatin added to the Zn (0.20 M)–Cit (0.25 M) bath, (c) concentration of Zn ions in the Cit (0.25 M)–Zn electrolyte, and (d) concentration of Cit ions in Cit–Zn (0.20 M) electrolyte.

Finally, Fig. 3d presents the influence of hydrodynamic conditions on the kinetics of the electrode processes in the Zn–Cit–SiC–gel system. It is evident that the process of hydrogen evolution at low polarization (Fig. 3d, inset I) depends on the RDE speed, while the current density associated with zinc deposition at polarization of –1.5 to –2.0 V vs. SCE (related current density values of up to –3.0 A dm^{-2}) is independent of the RDE speed. This implies that this reaction is activation-controlled. Further negative shift of potential results in the change of the kinetic regime, to diffusion-controlled. Also, the characteristic blockage of the cathode surface by hydrogen gas bubbles at high polarization and low RDE (150 rpm) is observed in the Zn–Cit–SiC–gel system.

In summary of this section, it is concluded that zinc deposition is possible in the presence of SiC NPs suspended in Zn–Cit electrolyte together with gelatin. Gelatin inhibits the reduction processes by adsorption on the cathode surface, while the addition of SiC seems to hinder, or almost eliminate, the effect of gelatin in the studied system. Such enhancement of the kinetics by the presence of NPs may be associated with the adsorption of gelatin and citrate ions on the surface of the ceramic NPs, thus changing their speed of transport to the cathode. To verify this hypothesis, zeta-potential measurements were performed; the results are described in the following section.

Zeta potential of SiC nanoparticles.—As evident from Fig. 4a, the zeta potential of SiC NPs suspended in pure deionized water is around –25 mV. This value is essentially unchanged when gelatin is added, implying that gelatin does not change the surface charge of SiC, i.e. gelatin does not interact with SiC in pure water. The addition of zinc ions in the absence of citrate and gelatin practically does not influence the measured zeta potential, whereas the addition of citrate ions to the H_2O–SiC system results in a slight change of the surface charge to a more negative value (–29 mV). The zeta potential of SiC NPs is most negative (–36 mV) in the Zn–Cit solution. These results clearly indicate the adsorption of negative citrate and zinc-citrate ions onto the surface of the SiC NPs, thus changing their surface charge.

Due to the very high molecular weight of gelatin, its content in the plating baths in the present study represents a concentration, which is several orders of magnitude smaller than the concentration of the zinc ions. Thus, gelatin could not act as a complexing agent. Gelatin can be regarded as an amphoteric surfactant due to the presence of both carboxylic and amino groups.[35] However, it shows cationic behavior at pH values below its isoelectric point (pH < 4.7–5.4), because of the protonation of amino groups.[35–37] Consequently, the addition of gelatin results in shift of the zeta potential to less negative values, regardless of whether the system is H_2O–Cit, H_2O–Zn, or H_2O–Cit–Zn (Fig. 4a). This is a proof of the adsorption of gelatin on the surface of the SiC NPs. The zeta potential of SiC increases with the increase of gelatin concentration in the Zn–Cit electrolyte, up to a limiting value of 1.5 g dm^{-3} (Fig. 4b). In contrast, the increase of the zinc ion (Fig. 4c) and citrate ion (Figs. 4d) concentrations in Zn–Cit electrolytes results in a noticeable decrease in the charge of the SiC surface, to more negative values, as long as all zinc and citrate ions are bound to each other in the form of Zn–Cit complex ions. Once there is excess of either free zinc ions or free citrate ions, the zeta potential starts to increase (to less negative values). The data presented in Figs. 4b, 4c, 4d is in line with the dependences shown in Fig. 4a and supports the adsorption of negative Cit and Zn–Cit ions as well as positive gelatin fragments on the surface of the SiC NPs in the studied electrolyte solutions.

Electrodeposition of Zn and Zn–SiC layers.—Galvanostatic DC electrodeposition of Zn–SiC composite layers from Zn–Cit–gel–SiC bath was studied and compared with that of pure Zn deposition from a Zn–Cit–gel electrolyte (Fig. 5). This comparison allows to better

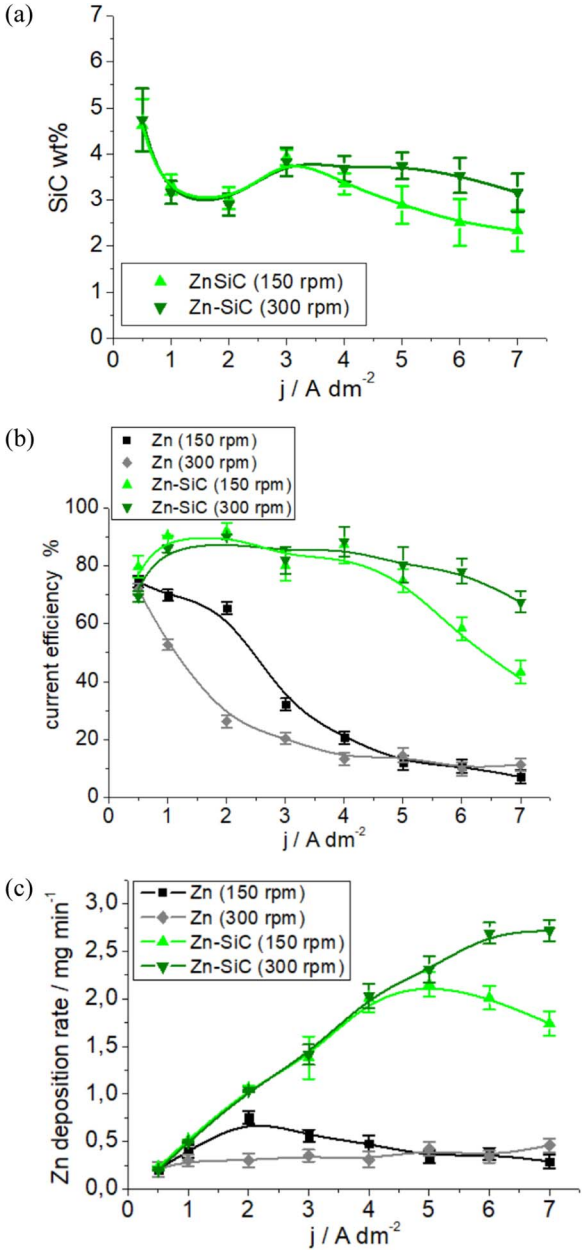

Figure 5. The effect of current density on (a) SiC content in Zn–SiC composite deposits, (b) the current efficiency of zinc electrodeposition, and (c) Zn deposition rate, in the presence or absence of SiC, at two chosen RDE speeds: $\omega_1 = 150$ rpm, $\omega_2 = 300$ rpm. Electrolyte composition: 0.25 M Cit, 0.20 M $ZnSO_4$, 1 g dm^{-3} gelatin, 60 g dm^{-3} SiC. $T = 20$°C, $Q = 20$ C.

understand the effect of suspended SiC NPs in solution. Figure 5a shows the dependence of the content of SiC incorporated into Zn deposit on the applied current density, whereas Fig. 5b and Fig. 5c show the dependences of current efficiency and zinc deposition rate, respectively.

From Figs. 5b, 5c it is evident that the addition of suspended SiC NPs has a significant effect on the kinetics of zinc deposition. This behavior is consistent with the results obtained from cyclic voltammetry (Figs. 2 and 3), and can be explained by the adsorption of gelatin molecules on the SiC particles (Fig. 4), which do not adsorb directly on the cathode, therefore undermining their inhibiting effect on the Zn reduction process. The dependence of the composition of Zn–SiC electrodeposits on the applied current density is twofold: (I) at smaller current densities (from –0.5 to –3.0 A dm^{-2}), the amount of the codeposited SiC is independent of the of velocity of the RDE (in the studied range of 150 to 300 rpm), and (II) at higher current densities (from –4.0 to –7.0 A dm^{-2}), the content of SiC in Zn–SiC deposits depends on mass transport limitation, and is noticeably higher for the higher RDE speed considered (i.e. 300 rpm), see Fig. 5. The observed phenomena can be associated with a change in the kinetic regime of the electrode processes, from activation controlled at smaller current densities (I) to diffusion-limited at higher current densities (II), as indicated by the voltammetric analysis too (Fig. 3d).

In part (I), where zinc deposition is controlled by charge transfer, the rate of codeposition of SiC NPs does not change considerably with the increase of the flux of the particles to the growing layer surface, as the RDE speed is increased from 150 to 300 rpm. Hence, no matter how many SiC particles surrounded by adsorbed Zn–Cit complexes reach the cathode surface, the SiC embedment rate is controlled by the rate of the Zn electrodeposition, which is independent of the mass transport rate under these conditions. At higher cathodic current densities, part (II), when the zinc deposition process is diffusion controlled, the increase of RDE speed leads to rise of SiC flux toward the cathode surface, thus resulting in the increase of SiC content codeposited with Zn (Fig. 5a), along with the increase of current efficiency (Fig. 5b) and Zn deposition rate (Fig. 5c). This implies that only SiC particles that are part of the reduction processes are incorporated into the zinc matrix, indicating that SiC codeposition takes place by the entrapment during the zinc electrodeposition from the Zn–Cit adsorbed on the SiC NPs. However, not all Zn–Cit ions in the electrolyte are expected to be bound with SiC NPs via adsorption; the zinc electrodeposition process may proceed through both the reduction of freely solvated Zn–Cit complex molecules from the bulk solution and Zn–Cit adsorbed on SiC. Therefore, the concentration of codeposited SiC is a result of the total growth rate of the depositing Zn film and the residence time of the particles on the growing surface.[2]

At higher cathodic currents, part (II), when the Zn deposition rate grows explicitly with the increase of applied current density (Fig. 5c), the Zn deposition rate increases, and the weight percent of SiC slightly decreases (Fig. 5a). Moreover, the hydrogen evolution rate generally increases significantly as the current density increases, which is reflected by a decrease in current efficiency (Fig. 5b). At current densities higher than –5.0 A dm^{-2}, the Zn deposition rate decreases only in the case of RDE speed of 150 rpm. This is associated with the intensive hydrogen evolution and the blockage of the cathode surface by the hydrogen gas bubbles remaining on its surface at the lowest RDE speed applied. At higher rotation rate, these bubbles are more easily "swept" from the surface, ensuring the continuity of the proceeding electrode reactions.

The dependences of SiC wt%, current efficiency, and Zn deposition rate at smaller current densities, part (I), are more complex, and can be divided into three subparts: $j = -0.5$ A dm^{-2}, j from –1.0 to –2.0 A dm^{-2}, and $j = -3.0$ A dm^{-2}. At $j = -0.5$ A dm^{-2}, the current efficiency (Fig. 5b) and Zn deposition rate (Fig. 5c) reach similar values for both the Zn–Cit–gel and Zn–Cit–gel–SiC systems. The current efficiency of pure zinc deposition process is the highest (Fig. 5b); the content of SiC codeposited with zinc also reaches a maximum (Fig. 5a). Such maxima of ceramic particles incorporation in electrodeposited metal matrices have been observed in the literature,[60–62] suggesting that they occur at the potential of zero charge (E_{pzc}).[60,61,63] The latter is defined as the potential at which the net surface charge density equals zero.[64] It was suggested that the short-range repulsive hydration force due to ordering of solvent molecules at interfaces in concentrated electrolytes is minimal if the electric field at the electrode is minimal (i.e., at E_{pzc}). This would enable ceramic particles to get closer to the electrode, so that the particles are attached to the growing deposit by dispersion forces.[61,62] Moreover, a maximum in the particle inclusion vs. current density could be caused by changes in the ordering of the water dipoles due to changes in electrode charge.[60,63] Left or right from the PZC, the electric field near the electrode increases, and the water dipoles line up, either flipped up or down according to the sign of the electric field.[60] Since SiC is hydrophobic, it would codeposit readily as long as it can be kept in suspension during electrolysis.

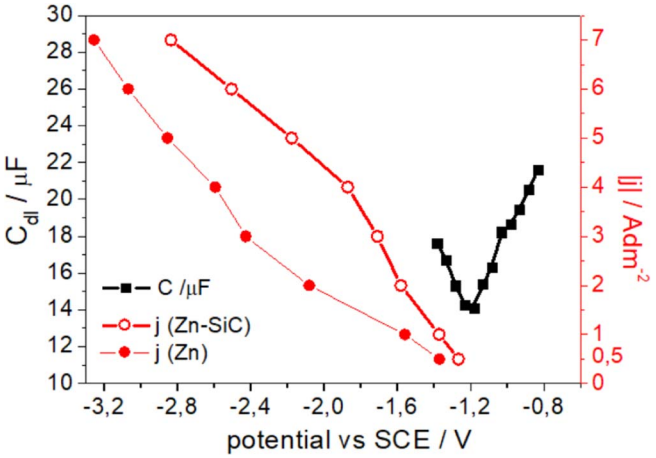

Figure 6. Double-layer capacitance vs. potential (black squares) and applied current density vs. resulting mean potential (red circles) measured during the galvanostatic Zn–SiC and Zn deposition referred to in Fig. 5.

Since E_{pzc} corresponds to the potential at which the double-layer capacitance C_{dl} reaches a minimum,[60,65,66] EIS measurements were performed to determine the values of C_{dl} and estimate E_{pzc} in the studied system. Fig. 6 shows the C_{dl} vs. potential curve compared with the dependence of the deposition current density and associated potential values. A minimum in C_{dl} is evident at about –1.20 V vs. SCE. This value of E_{pzc} coincides with the overpotential registered during galvanostatic Zn and Zn–SiC deposition at $j = –0.5$ A dm^{-2}, thus confirming that the maximum in the codeposition of SiC is linked to the E_{pzc} (Figs. 5a and 6). Furthermore, no adsorption of gelatin occurs on the cathode at E_{pzc}, which could explain the same kinetics of Zn electrodeposition at $j = –0.5$ A dm^{-2} in both Zn–Cit–gel and Zn–Cit–gel–SiC systems (Figs. 5b, 5c).

At cathodic current densities higher than $j = –0.5$ A dm^{-2}, the working electrode begins to be polarized negatively. However, both citrate-based complex ions and SiC NPs are also negatively charged (Figs. 1 and 4), hence their migration to the cathode cannot be explained by a simple electrostatic attraction. These phenomena are commonly known, and it is considered that the electrodeposition of metals mainly proceeds on the cathode through the multistep reduction of negatively charged ions. These complex anions approach the cathode by convection and/or diffusion, while specific adsorption effects can occur in the double layer.[67] The mechanism explaining those phenomena is still not fully understood. Here, it is only essential to state that SiC particles surrounded by adsorbed Zn–Cit ions are expected to be attracted to the cathode surface by the same force as freely solvated Zn–Cit ions. On the other hand, mass transport from the bulk can also be affected by the presence of solid ceramic particles suspended in the electrolyte. It is commonly considered that solid particles dispersed in a liquid may enhance the convective mass transport. It was shown[68–70] that solid particles in the electrolyte may establish local "micro-convective" flows (resulting from the rotation of solid particles), which superimpose on the bulk flow field. Furthermore, the rotation of the particles in the diffusion layer causes a decrease of the average diffusion layer thickness, while the value of the diffusion coefficient is expected to be unaffected by the particles. However, it should be noted that, in cases used to create the abovementioned model, the particles were not incorporated into the electrodeposited layer, but were only swept toward the cathode surface. In contrast, herein the SiC particles embed into the zinc coating. SiC is known for its electrical semiconductor properties,[71,72] yet it has a comparatively much higher resistivity than the zinc matrix. Consequently, higher nucleation overpotential and lower charge transfer rate are expected on the surface of adsorbed SiC particles.

The opposite effect, observed in the Zn–Cit–SiC system, can be explained by the fact that Zn–Cit ions adsorb on the SiC NPs in the electrolyte solution. Thereby, the SiC NPs adsorbing on the cathode surface are the carrier of electroactive Zn–Cit ions, which undergo an electroreduction process while SiC particles are entrapped in the deposited layer.

Furthermore, at cathodic current densities higher than $j = –0.5$ A dm^{-2}, the current efficiency of pure zinc deposition drops sharply due to inhibition of the process by the adsorption of the gelatin on the cathode surface. Interestingly, the effect of a decrease of the RDE rotation rate on pure zinc electrodeposition, at current densities from –1.0 to –3.0 A dm^{-2}, results in an increase of both zinc deposition rate and current efficiency.

It has been claimed by Kazimierczak et al.[51] that zinc reduction from citrate complexes occurs in two separate steps. Therefore, Eqs. 4 and 5 from Electrode reactions in the Zn–Cit system section can be presented in two steps. The first step occurs according to the outer-sphere charge transfer mechanism: Zn(II) is reduced to Zn(I), leading to the formation of a Zn(I)-citrate complex adsorbed on the surface of the cathode, Eqs. 4a and 5a. The adsorbed citrate complex of zinc can be reduced further to Zn, according to an inner-sphere charge transfer mechanism, Eqs. 4b and 5b:

$$Zn(HCit)^- + e^- \rightarrow (ZnHCit_{ads})^{2-} \qquad \text{(4a, outer-sphere)}$$

$$(ZnHCit_{ads})^{2-} + H_2O + e^- \rightarrow Zn^0 + (H_2Cit)^{2-} + OH^- \qquad \text{(4b, inner-sphere)}$$

$$ZnH_2Cit^0 + e^- \rightarrow (ZnH_2Cit_{ads})^- \qquad \text{(5a, outer-sphere)}$$

$$(ZnH_2Cit_{ads})^- + e^- \rightarrow Zn^0 + H_2Cit^{2-} \qquad \text{(5b, inner-sphere)}$$

In these equations, the designation Cit^{4-} is used for the citrate anion, thus representing the fully deprotonated form of citric acid (H_4Cit, or $C_6H_8O_7$). This designation eliminates the necessity to describe the deprotonated citrate ion as $H_{-1}Cit^{4-}$, which is the case when using the Cit^{3-} designation.[73] In inner-sphere charge transfer reactions, the reactants are in direct contact with each other, without any intervening solvent molecules. The reactants get coupled so tightly to each other during the reaction, forming an activated complex, which can be regarded as a 'single' entity. In the case of metal complexes, the main energy changes connected to the electron transfer are ascribed to a variation in the bond lengths or angles between the metal and the ligands. In contrast, in outer-sphere charge transfer reactions, the reactants are separated from each other by some solvent molecules due to the solvation of the reactants. Outer-sphere mechanisms require that the reactants become so close to each other that the first solvation spheres touch each other. Then, a so-called electron hopping is possible.[74]

A sufficiently long residence time of adsorbed citrate complexes of Zn(I) is necessary for Zn deposition at low polarization, where Reactions 4 and 5 are relatively slow. The decrease of Zn deposition rate and current efficiency with the increase of rotation rate suggests that the Zn(I) species formed by outer-sphere charge transfer reactions may be more easily removed from the cathode surface when the RDE speed is increased. A deeper understanding and confirmation of this theory requires further research, which is behind the scope of the work presented herein. It is suffice to note that at current densities of up to –3.0 A dm^{-2}, a decrease of the RDE speed results in a slight increase of both the Zn deposition rate and current efficiency (Fig. 5b).

The changes in the amount of SiC codeposited with zinc at current densities from –1.0 to –2.0 A dm^{-2} and the value registered at –3.0 A dm^{-2} (Fig. 5a) may be related to the difference in the standard potentials of the two reactions expressed in Eqs. 4 and 5, and consequently, the sequence of reduction reactions.

It was shown before[51] that ZnH_2Cit^0 and $Zn(HCit)^-$ do not react with one another, and that they are reduced on the cathode independently of each other, one after the other. At lower polarization (less negative than –1.7 V vs. SCE), only the ZnH_2Cit complex, which

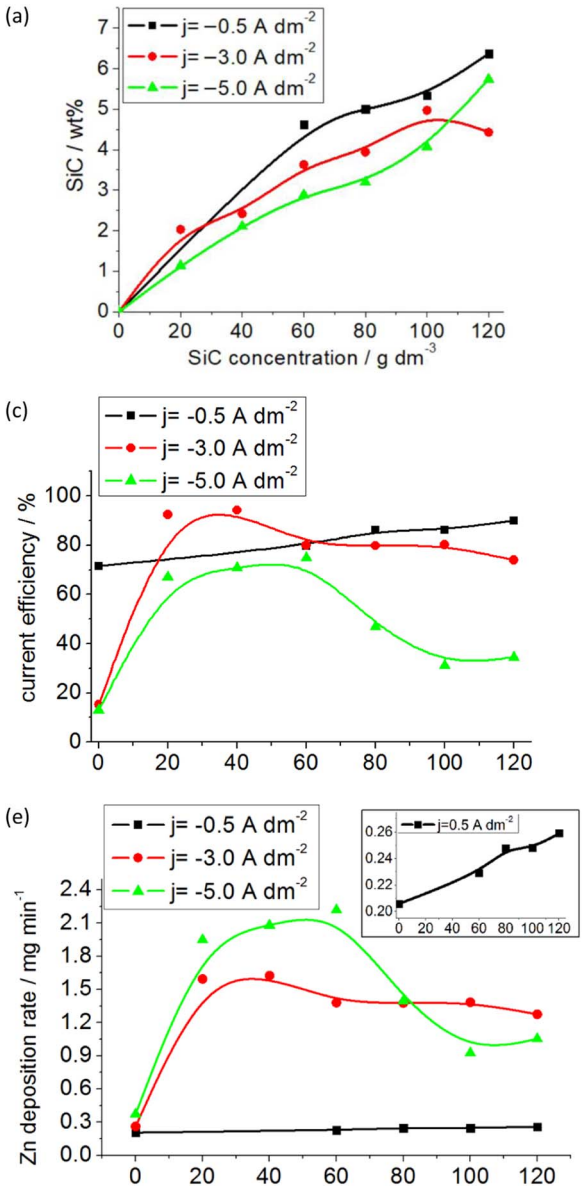

Figure 7. The effect of SiC concentration in electrolyte on (a) SiC content in Zn–SiC composite deposits, (b) the current efficiency of zinc electrodeposition, and (c) Zn deposition rate. Electrolyte composition: 0.25 M Cit, 0.20 M $ZnSO_4$, 1 g dm^{-3} gelatin. ω = 150 rpm, Q = 20 C, T = 20°C.

exists at lower concentrations (Fig. 1), is reduced. In contrast, at potentials more negative than –1.7 V, reduction of both ZnH_2Cit^0 and $Zn(HCit)^-$ takes place. This can clearly be related to the phenomena observed during electrodeposition in the Zn–SiC system. When Zn–SiC is electrodeposited at –1.0 to –2.0 A dm^{-2}, the registered cathodic overpotential does not exceed –1.6 V vs. SCE (Fig. 6), and the concentration of codeposited SiC is about 3 wt%. The overpotential when applying –3.0 A dm^{-2} is –1.72 V vs. SCE, and the content of incorporated SiC increases to about 4 wt% (Fig. 5a). Thus, if both ZnH_2Cit^0 and $Zn(HCit)^-$ ions are adsorbed on the SiC particles, and the SiC codeposition takes place via entrapment of ceramic particles during the zinc electrodeposition from Zn–Cit adsorbed on its surface, then under conditions when more $(Zn–Cit)_{ads}SiC$ ions can be reduced (i.e., at j = –3.0 A dm^{-2}), the probability of SiC entrapment in the growing Zn matrix is the highest.

Fig. 7 shows the effect of the concentration of SiC NPs suspended in the electrolyte on the Zn–SiC codeposition process at three selected current densities of –0.5, –3.0, and –5.0 A dm^{-2}. The lowest rotation rate (150 rpm) was chosen here due to the fact that the attraction of SiC particles and Zn–Cit molecules to the cathode surface and their residence time seem to be favourable under such hydrodynamic conditions. In all three cases, the amount of SiC codeposited with Zn increases with the increase of the SiC concentration in the electrolyte (Fig. 7a). At –0.5 A dm^{-2}, where Zn–SiC codeposition is the slowest, codeposition of SiC proceeds only via the reduction of ZnH_2Cit^0, and is related to E_{pzc}. Thus, the increase of the weight percent of SiC incorporated into the Zn matrix is clearly related to the increase of Zn deposition rate (Fig. 7c), and consequently – to current efficiency (Fig. 7b). This confirms that, under such conditions, zinc deposition occurs mainly through the reduction of ZnH_2Cit^0 ions adsorbed on SiC. Therefore, the increasing amount of SiC NPs attracted to the cathode surface does not hinder, but actually enhances, the electrodeposition process.

At –3.0 A dm^{-2}, the reduction of Zn is significantly faster, proceeding largely through the reduction of freely solvated Zn–Cit ions. Therefore, the increasing concentration of SiC adsorbed on the cathode results in a slight decrease of both current efficiency and Zn deposition rate (Figs. 7b, 7c). At higher RDE speeds (not shown here), such a decrease of current efficiency was not observed, possibly because the responsible species is swept from the cathode surface. Therefore, the above phenomena may be related to the blockage of the flux of freely solvated Zn–Cit ions to the cathode surface in the presence of a growing concentration of SiC in its vicinity. The hydrogen evolution rate is not significant under such conditions. However, pure citrate ions, which result from relatively fast zinc reduction processes, Eqs. 4 and 5, may remain in the vicinity of the cathode surface, thus inhibiting the zinc reduction process. Consequently, all the phenomena observed during the Zn–SiC electrodeposition at j = –3.0 A dm^{-2} are the result of overlapping of all processes described above. Namely, the two main processes taking place simultaneously: reduction of Cit–Zn ions adsorbed on SiC NPs, and Zn reduction from the freely solvated Cit–Zn ions. The latter is hindered by the excess of SiC and citrate ions remaining in the vicinity of the cathode surface.

At –5.0 A dm^{-2}, the aforementioned hindering of zinc deposition due to increasing concentration of SiC is more pronounced, and results in the pronounced decrease of current efficiency and zinc deposition rate when the concentration of SiC suspended in the electrolyte exceeds 60 g dm^{-3}. This can be associated with the fact that, under such conditions, both zinc deposition and hydrogen evolution processes are relatively fast, and the hydrogen gas bubbles remain on the cathode surface and block it. Additionally, SiC is considered a catalyst for hydrogen evolution,[75,76] thus the higher is the amount of SiC on the cathode – the faster is the hydrogen evolution process. Moreover, SiC at higher concentration is more likely to form agglomerates, while intensive hydrogen evolution leads to the formation of porous and rough electrodeposits; hence, SiC NPs are more likely to be mechanically entrapped in large clusters, thus blocking the cathode more easily.

SEM characterization of Zn–SiC deposits.—SEM images of the cross-section of Zn–SiC layers electrodeposited from baths containing different concentrations of SiC are shown in Fig. 8. This figure confirms that SiC particles are incorporated into the Zn matrix. In addition, it can be noticed that the increase of the concentration of suspended SiC in the bath leads to more agglomeration of NPs and their entrapment as aggregates.

SEM images at high magnification reveal that SiC is not only incorporated into the Zn matrix in the form of agglomerates, but there are also small individual SiC particles distributed in the volume of each coating. It should also be mentioned that the structure may contain some cavities in the Zn matrix. Hence, it is very important to differentiate between pores and particles. Cavities yield various contrasts in an image, but their compositions are the same as the matrix. Fig. 9 shows the cross-section of a chosen Zn–SiC coating, with marked crosses where local chemical analysis was conducted. The limited resolution of the SEM-EDS microanalysis (of about 1 μm) and the presence of either individual SiC NPs or their agglomerates close to each other might affect the results. Nonetheless, the considerable

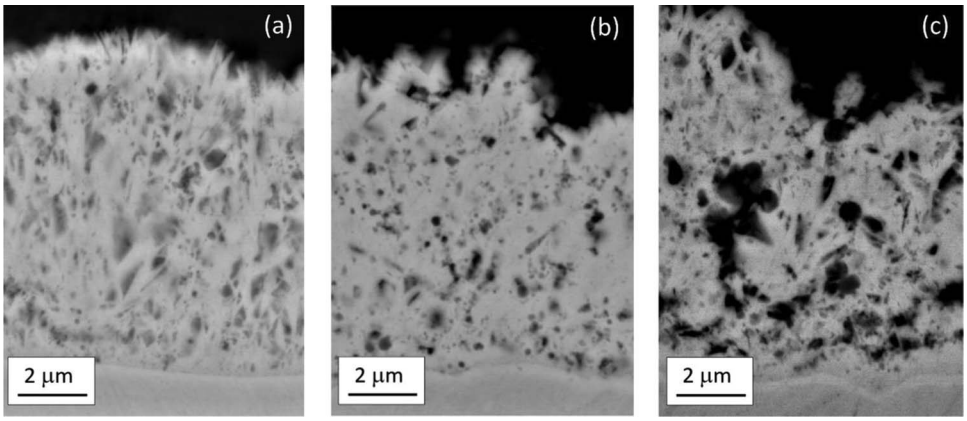

Figure 8. SEM backscatter electron (BSE) images of cross-sections of Zn–SiC layers electrodeposited at $j = -3.0$ A dm^{-2} from baths containing different concentrations of SiC: (a) 60 g dm^{-3}, (b) 80 g dm^{-3}, (c) 100 g dm^{-3}, $\omega = 350$ rpm, $Q = 80$ C, $T = 20°$C.

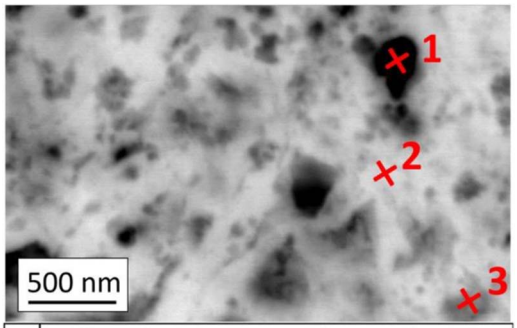

	Si wt%	Zn wt.%	C wt%
1	7.2 ± 0.3	89,8 ± 0.9	3.1 ± 0.6
2	0.5 ± 0.5	99.3 ± 0.7	0.2 ± 0.2
3	2.0 ± 0.4	97.2 ± 1.2	0.8 ± 0.8

Figure 9. SEM BSE image of a cross-section of a Zn-SiC layer electrodeposited at $j = -3.0$ A dm^{-2} from an electrolyte solution containing 80 g dm^{-3} SiC. The local chemical composition (EDS) at the three marked crosses is given below the figure. $\omega = 350$ rpm, $Q = 80$ C, $T = 20°$C.

differences observed in the composition at various characteristic points in the cross-section of the coating confirm that the black and dark gray spots visible in the cross-section are enriched with SiC.

Conclusions

- Pure zinc and Zn–SiC composite coatings were successfully electrodeposited from aqueous citrate solutions at pH = 4.5 under constant direct current conditions within the current density range of –0.5 to–7.0 A dm^{-2}.
- Zeta potential measurements confirmed the adsorption of citrate and citrate-zinc ions on the surface of the SiC NPs.
- SiC incorporation behavior as a function of current density can be described by several regions: (1) a region where the SiC content in Zn–SiC deposits reaches a maximum (explained by the condition of potential of zero charge), (2) a region with a pronounced decline in incorporation, followed by its slight increase (related to the activation-controlled reduction of ZnH_2Cit^0 and $Zn(HCit)^-$ ions adsorbed on SiC NPs, respectively), and (3) a region with another decrease of SiC incorporation together with current density increase (which is linked to mass transport-limited conditions and intensive hydrogen evolution).
- A scheme describing the mechanism of electrode reactions occurring in the studied Zn–Cit and Zn–Cit–SiC systems is proposed. It is shown that SiC codeposition with Zn proceeds through the entrapment of ceramic NPs during the reduction of citrate-zinc ions firstly adsorbed on their surface, which can be schematically described by either inner-sphere or outer-sphere charge transfer reactions:

$$Zn(HCit)^- + SiC \rightarrow Zn(HCit)^-_{ads}\,(SiC) \quad [11]$$

$$Zn(HCit)^-_{ads}\,(SiC) + H_2O + 2e^- \rightarrow Zn - SiC + H_2Cit^{2-} + OH^- \quad [12]$$

$$ZnH_2Cit^0 + SiC \rightarrow ZnH_2Cit^0_{ads}\,(SiC) \quad [13]$$

$$ZnH_2Cit^0_{ads}\,(SiC) + 2e^- \rightarrow Zn - SiC + H_2Cit^{2-} \quad [14]$$

- Zinc electrodeposition may proceed either via the reduction of freely solvated Zn–Cit complex molecules from the bulk of the solution or via Zn–Cit adsorbed on SiC NPs. Therefore, the concentration of codeposited SiC is a result of the total growth rate of the depositing Zn film and the residence time of the NPs on the growing surface, which changes when the electrode kinetics control (activation or diffusion) is changed under the chosen current/potential conditions.
- The content of SiC NPs in the coating is influenced by current density, RDE speed, and SiC NPs concentration in the electrolyte solution. The maximum SiC content of 6.4 wt% in the Zn coating was obtained when the SiC NPs concentration in the plating bath was 120 g dm^{-3}, the current density was –0.5 A dm^{-2}, and the RDE speed was 150 rpm. The current efficiency of the electrodeposition process was maintained at around 90%.
- SEM observation confirmed the incorporation of SiC NPs into the volume of the Zn matrix layer, both in the form of agglomerates of various sizes and as individual SiC particles.

Acknowledgments

The research was initiated and mainly conducted within the framework of project No. LIDER/007/151/L-5/13/NCBR/2014 financed by the National Centre for Research and Development in Poland. The cooperation between the Institute of Metallurgy and Materials Science of the Polish Academy of Sciences and Tel-Aviv University was enabled thanks to COST Action MP1407 (e-MINDS). The authors gratefully acknowledge Dr. Remigiusz Kowalik for the possibility to carry out WDXRF measurements at AGH University of Science and Technology (Krakow, Poland), and Dr. Piotr Bobrowski for SEM observations at the Institute of Metallurgy and Material Science, Polish Academy of Sciences (Krakow, Poland).

ORCID

Honorata Kazimierczak https://orcid.org/0000-0001-9152-0041
Noam Eliaz https://orcid.org/0000-0002-1184-4706

References

1. N. Eliaz and E. Gileadi, *Physical Electrochemistry: Fundamentals, Techniques, and Applications*, 2nd ed., ISBN: 978-3-527-34139-9, Wiley-VCH, Germany (2010).
2. P. M. Vereecken, I. Shao, and P. C. Searson, *J. Electrochem. Soc.*, **147**, 2572 (2000).
3. V. B. Singh and D. K. Singh, *Nanosci. Technol.*, **1**, 1 (2014).
4. F. C. Walsh and C. Ponce de Leon, *Trans. Inst. Metal Finish.*, **92**, 83 (2014).
5. P. Nowak, R. P. Socha, M. Kaisheva, J. Fransaer, J.-P. Celis, and Z. Stoinov, *J. Appl. Electrochem.*, **30**, 429 (2000).
6. L. Benea, P. L. Bonora, A. Borello, and S. Martelli, *Wear*, **249**, 995 (2002).
7. S. C. Wang and W. C. J. Wei, *J. Mater. Res.*, **18**, 1566 (2003).
8. H. Wang, S. Yao, and S. Matsumara, *J. Mater. Process. Technol.*, **145**, 299 (2004).
9. M. D. Ger, *Mater. Chem. Phys.*, **87**, 67 (2004).
10. H. K. Lee, H. Y. Lee, and J.-M. Jeon, *Surf. Coat. Technol.*, **201**, 4711 (2007).
11. P. Gyftou, E. A. Pavlatou, and N. Spyrellis, *Appl. Surf. Sci.*, **254**, 5910 (2008).
12. I. Dobosz, E. Rudnik, and L. Burzynska, *Arch. Metall. Mater.*, **56**, 665 (2011).
13. F. Kilic, H. Gul, S. Aslan, A. Alp, and H. Akbulut, *Colloids Surf. A*, **419**, 53 (2013).
14. Y. H. Ahmad and A. M. A. Mohamed, *Int. J. Electrochem. Sci.*, **9**, 1942 (2014).
15. S. P. Devaneyan and T. Senthilvelan, *Proced. Eng.*, **97**, 1496 (2014).
16. W. Q. Liu, W. N. Lei, C. Ye Wang, H. F. Qian, and L. H. Ding, *Integr. Ferroelectr.*, **167**, 192 (2015).
17. C Müller, M. Sarret, and M. Benballa, *Surf. Coat. Technol.*, **162**, 49 (2003).
18. P. C. Tulio, S. E. B. Rodrigues, and I. A. Carlos, *Surf. Coat. Technol.*, **202**, 91 (2007).
19. P. C. Tulio and I. A. Carlos, *J. Appl. Electrochem.*, **39**, 1305 (2009).
20. G. Roventi, T. Bellezze, and R. Fratesi, *J. Appl. Electrochem.*, **43**, 839 (2013).
21. M. Sajjadnejad, H. Omidvar, M. Javanbakht, R. Pooladi, and A. Mozafari, *Trans. Inst. Met. Finish.*, **92**, 227 (2014).
22. M. Sajjadnejad, A. Mozafari, H. Omidvar, and M. Javanbakht, *Appl. Surf. Sci.*, **300**, 1 (2014).
23. M. K. P. Kumar, T. V. Venkatesha, and M. K. Pavithra, *Int. J. Electrochem. Sci. Eng.*, **5**, 25 (2015).
24. N. Haghmoradi, C. Dehghanian, and S. Yari, *JMEPEG*, **25**, 3746 (2016).
25. G. Roventi, G. Giuliani, M. Pisani, and T. Bellezze, *Int. J. Electrochem. Sci.*, **12**, 663 (2017).
26. C. T. J. Low, R. G. A. Wills, and F. C. Walsh, *Surf. Coat. Technol.*, **201**, 371 (2006).
27. L. Benea, P. L. Bonora, A. Borello, S. Martelli, F. Wenger, P. Ponthiaux, and J. Galland, *J. Electrochem. Soc.*, **148**, C461 (2001).
28. R. P. Socha, P. Nowak, K. Laajalehto, and J. Väyrynen, *Colloids Surf. A*, **235**, 45 (2004).
29. E. C. Lee and J. W. Choi, *Surf. Coat. Technol.*, **148**, 234 (2001).
30. S. H. Yeh and C. C. Wan, *J. Appl. Electrochem.*, **24**, 993 (1994).
31. J. Drzymała, *Int. J. Mineral Process.*, **42**, 153 (1994).
32. N. Guglielmi, *J. Electrochem. Soc.*, **119**, 1009 (1972).
33. B. J. Hwang and C. S. Hwang, *J. Electrochem. Soc.*, **140**, 979 (1993).
34. D. Erogluz and A. C. West, *J. Electrochem. Soc.*, **160**, D354 (2013).
35. S. K. Samal, M. Dash, S. Van Vlierberghe, D. L. Kaplan, E. Chiellini, C. van Blitterswijk, L. Moroni, and P. Dubruel, *Chem. Soc. Rev.*, **41**, 7147 (2012).
36. X. Xia, I. Zhitomirsky, and J. R. McDermid, *J. Mater. Process. Technol.*, **209**, 2632 (2009).
37. N. Sahoo, R. K. Sahoo, N. Biswas, A. Guha, and K. Kuotsu, *Int. J. Biolog. Macromolecules*, **81**, 317 (2015).
38. L. D. Pettit and K. J. Powell, The IUPAC stability constants database, SC-Database for Windows, Academic Software, Release 5, Sourby Old Farm, Timble, Otley, Yorks, UK (2012).
39. WATEQ4F – Revised Thermodynamic Database, The United States Geological Survey (USGS) Open-File Report 1991-183 (1991).
40. W. R. Smith and R. W. Missen, *Chemical Reactions Equilibrium Analysis: Theory and Algorithms*, John Wiley & Sons, Toronto (1982).
41. WATEQ4F Database, The United States Geological Survey (USGS), Open-File Report 91–183 (2001).
42. P. Ozga, *Influence of complex formation on electrodeposition of metals and alloys from citrate solutions (in Polish)*, IMMS PAS, Krakow, Poland (2006).
43. P. Ozga, *The thermodynamic models of complex electrolytic baths for electrodepostion of zinc and tin alloys (in Polish)*, 2006–2010, Polska Metalurgia w latach. Krakow: Akapit (2010).
44. P. Ozga, Z. Świątek, A. Dębski, J. Bonarski, L. Tarkowski, E. Bielańska, P. Handzlik, B. Onderka, and M. Michalec, *Modern technologies and advanced materials and products in balanced development of non-ferrous metals industry (in Polish)*, IMN Gliwice, ISBN 978-83-925546-6-0 (2010).
45. I. Puigdomenech, *MEDUSA (Make Equilibrium Diagrams Using Sophisticated Algorithms) Program*, version 26, Royal Institute of Technology, Stockholm, Sweden (2009).
46. R. J. Hunter, *Zeta Potential in Colloid Science*, Academic Press, New York (1981).
47. M. Pushpavanam and K. Balakrishnan, *J. Appl. Electrochem.*, **26**, 1065 (1996).
48. H. Kazimierczak, P. Ozga, A. Jalowiec, and R. Kowalik, *Surf. Coat. Technol.*, **240**, 311 (2014).
49. H. Kazimierczak, P. Ozga, M. Slupska, Z. Swiatek, and K. Berent, *J. Electrochem. Soc.*, **161**, D309 (2014).
50. H. Kazimierczak and P. Ozga, *Surf. Sci.*, **607**, 33 (2013).
51. H. Kazimierczak, P. Ozga, and R. P. Socha, *Electrochim. Acta*, **104**, 378 (2013).
52. S. Krongelb, C. Bonhote, S. R. Brankovic, H. H. Gatzen, Y. Kitamoto, T. Osaka, W. Schwarzacher, and G. Zangari, Magnetic Materials, Processes and Devices 10, *ECS Trans*. **16**(45) (2010).
53. V. Marinovic and A. R. Despic, *J. Electroanal. Chem.*, **431**, 127 (1997).
54. I. W. Siriwardane, *Adsorption of citric acid on cerium oxide nanoparticles (nanoceria): effects of pH, surface charge and aggregation*, *MSc Thesis*, University of Iowa(2012).
55. M. Spasojevic, D. Gospavic, and M. Spasojevic, *J. Electrochem. Soc.*, **163**, D842 (2016).
56. M. R. Noerpel and J. J. Lenhart, *J. Colloid Interf. Sci.*, **460**, 36 (2015).
57. A. M. N. Silva, X. Kong, and R. C. Hider, *BioMetals*, **22**, 771 (2009).
58. K. Boto, *Electrodep. Surf. Treat.*, **3**, 77 (1975).
59. N. Eliaz, K. Venkatakrishna, and A. C. Hegde, *Surf. Coat. Technol.*, **205**, 1969 (2010).
60. J. Fransaer, J. P. Celis, and J. R. Roos, *J. Electrochem. Soc.*, **139**, 413 (1992).
61. J. L. Stojak and J. B. Talbot, *J. Electrochem. Soc.*, **146**, 4504 (1999).
62. N. L. Bengoa, P. Pary, and W. A. Egli, *J. Electrochem. Soc.*, **163**, D780 (2016).
63. A. Hovestad and L. J. J. Janssen, *J. Appl. Electrochem.*, **25**, 519 (1995).
64. M. Kosmulski, *Surface Charging and Points of Zero Charge*, CRC Press, Boca Raton, FL (2009).
65. K. Shimizu, J. Nyström, P. Geladi, B. Lindholm-Sethson, and J.-F. Boily, *Phys. Chem. Chem. Phys.*, **17**, 11560 (2015).
66. V. D. Jovic and B. M. Jovic, *J. Electroanal. Chem.*, **542**, 1 (2003).
67. M. Shwartz, Deposition from aqueous solutions, in: R. F. Bunshah, *Handbook of Deposition Technologies for Films and Coatings. Science, Technology and Applications*, 2nd ed., Park Ridge, New Jersey (1994).
68. P. K. Andersen, R. H. Muller, and C. W. Tobias, *J. Electrochem. Soc.*, **136**, 390 (1989).
69. P. J. Sonneveld, W. Visscher, and E. Barendrecht, *J. Appl. Electrochem.*, **20**, 563 (1990).
70. O. N. Sara, F. Icer, S. Yapici, and B. Sahin, *Exp. Term. Fluid. Sci.*, **35**, 558 (2011).
71. S. W. Watson, *J. Electrochem. Soc.*, **140**, 2235 (1993).
72. N. Kondrath and M. K. Kazimierczuk, *Int. J. Electronics Telecomunic.*, **56**, 231 (2010).
73. N. Eliaz and E. Gileadi, Induced codeposition of alloys of tungsten, molybdenum and rhenium with transition metals, Chapter 4, in *Modern Aspects of Electrochemistry*, Vol. **42**, eds. C. G. Vayenas, R. E. White, and M. E. Gamboa-Aldeco, Springer, New York (2008) pp. 191.
74. R. Seeber, C. Zanardi, and G. Inzelt, *ChemTexts*, **1**, 18 (2015).
75. C. He, X. Wu, J. Shen, and P. K. Chu, *Nano. Lett.*, **12**, 1545 (2012).
76. I. Lauermann, R. Memming, and D. Meissner, *J. Electrochem. Soc.*, **144**, 73 (1997).